Title

In-situ studies on martensitic transformation and high-temperature shape memory in small volume zirconia

Authors

Zeng, Xiao Mei
Du, Zehui
Tamura, Nobumichi
et al.

Publication Date

2017-08-01

DOI

10.1016/j.actamat.2017.06.006

Peer reviewed

Acta Materialia 134 (2017) 257–266

Contents lists available at ScienceDirect

Acta Materialia

journal homepage: www.elsevier.com/locate/actamat

Full length article

In-situ studies on martensitic transformation and high-temperature shape memory in small volume zirconia

Xiao Mei Zeng [a, b], Zehui Du [a], Nobumichi Tamura [c], Qing Liu [a], Christopher A. Schuh [d, 1], Chee Lip Gan [a, b, *]

[a] Temasek Laboratories, Nanyang Technological University, Singapore, 637553, Singapore
[b] School of Materials Science and Engineering, Nanyang Technological University, Singapore, 639798, Singapore
[c] Advanced Light Source (ALS), Lawrence Berkeley National Laboratory (LBNL), Berkeley, CA, 94720, USA
[d] Department of Materials Science and Engineering, Massachusetts Institute of Technology, 77 Massachusetts Ave, Cambridge, MA 02139, USA

ARTICLE INFO

Article history:
Received 23 March 2017
Received in revised form
1 June 2017
Accepted 5 June 2017
Available online 6 June 2017

Keywords:
Austenite-to-martensite phase transformation
X-ray synchrotron radiation
Shape memory effect (SME)
High temperature deformation
High temperature shape memory ceramics

ABSTRACT

Recently, the shape memory effect with significant recoverable shape deformation has been discovered in small volume single-crystal zirconia. The application potential for such shape memory ceramics has spurred in-depth exploration of the martensitic transformation crystallography and high temperature shape memory effect. In this work, the martensitic transformation of micron-sized zirconia has been studied in both a pristine as-produced condition and after micromechanical compression, using synchrotron scanning micro X-ray diffraction (μXRD). The pristine zirconia was found to transform into the monoclinic phase via a different crystallographic path than the compressed zirconia, resulting in distinct monoclinic variant preferences. The characteristic martensitic transformation temperatures were also found to be higher after uniaxial compression than in the pristine condition. Such observations provide insight on the differences between stress-induced and thermally-induced martensitic transformation. Moreover, we have observed a full cycle of the shape memory effect with large recoverable strain (7%) in micron-sized zirconia at a temperature of 400 °C. Our findings provide an important guideline to tailor the high-temperature shape memory properties of zirconia for further scientific research and engineering applications.

1. Introduction

The stress-induced shape memory effect [1], which originates from the martensitic transformation between austenite and martensite phases [2], has been extensively studied in metallic alloys at various operation temperatures [3–5]. The ability to experience significant shape deformation and recovery has made shape memory materials highly attractive for military, medical, aerospace and robotics applications [6–8]. Recently we reported a new class of shape memory ceramics: micron-sized single-crystal zirconia [9]. These ceramics exhibit strains comparable to metals but have higher strength and potentially higher operating temperatures than metals [10,11] for applications like solid state actuators [12]. The microscale single crystal structure, characterized by a large surface area-to-volume ratio and absence of grain boundaries, helps to accommodate transformation-induced stress and thus eliminate cracks [13–15]. As a result, small volume form factors enable the occurrence of stress-induced martensitic transformation between the tetragonal and monoclinic phases in zirconia, with a significant attendant shape change [10,11].

The martensitic transformation can be induced by external stress or by temperature change [4]. Therefore, the characteristic martensitic transformation temperatures [16] are expected to determine the operating temperature window of shape memory ceramics [12], and lay the foundation for tailoring their high temperature shape memory properties [17]. More importantly, our earlier work suggested that the stress-induced transformation in small volume zirconia could exhibit a systematic monoclinic variant preference in terms of transformation crystallography [18].

* Corresponding author.
E-mail addresses: xmzeng@ntu.edu.sg (X.M. Zeng), duzehui@ntu.edu.sg (Z. Du), ntamura@lbl.gov (N. Tamura), liuqing@ntu.edu.sg (Q. Liu), Schuh@mit.edu (C.A. Schuh), clgan@ntu.edu.sg (C.L. Gan).

[1] Prof. Christopher A. Schuh was an editor of the journal during the review period of the article. To avoid a conflict of interest, Prof. Greg Rohrer acted as editor for this manuscript.

http://dx.doi.org/10.1016/j.actamat.2017.06.006
1359-6454/

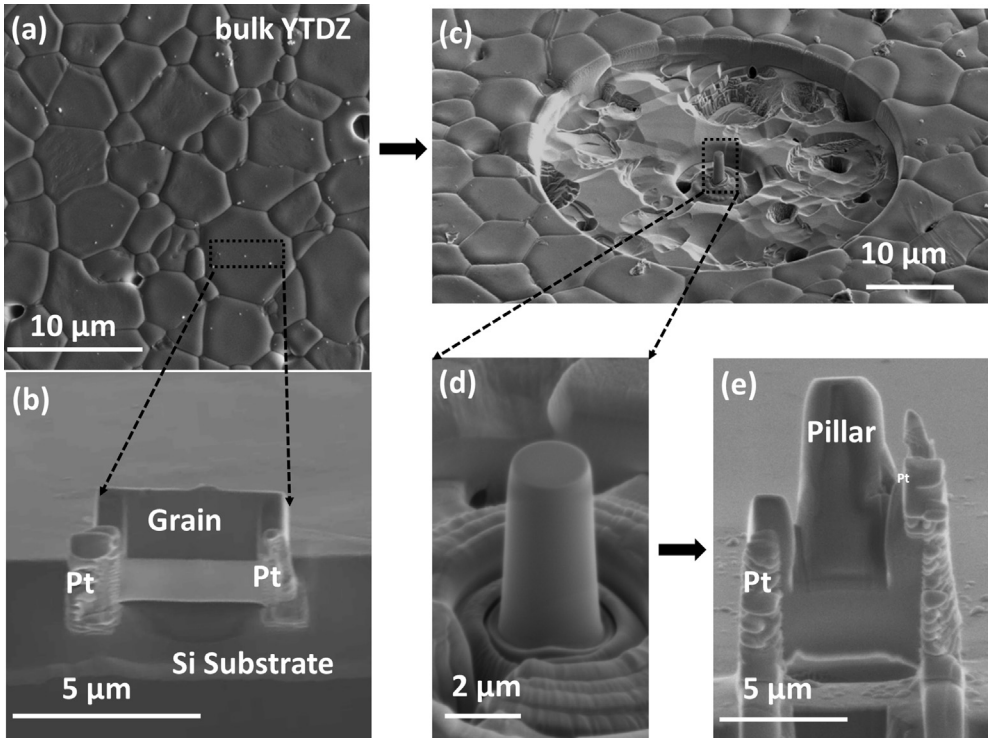

Fig. 1. (a) Grain structure of bulk yttria-titania doped zirconia (YTDZ). (b) Micron-sized grain mounted on a silicon substrate with Pt deposition. (c) Large crater milled on bulk YTDZ, surrounding (d) the pillar, with a viewing angle of 52°. (e) Compressed Pillar 3 mounted on a silicon substrate with Pt deposition.

On the other hand, if the transformation is triggered thermally without an externally applied stress to bias the variant selection, there are more degrees of freedom and variant competition may occur. In very small volume specimens, we envision that only a single variant would be plausibly supported, but it is unclear what factors would dominate the variant selection. Surface effects, residual stresses and defect substructure could all play a role, but there has been no prior exploration of variant selection for the thermally induced transformation in small volume shape memory ceramics. This is at least partly because the study of thermally-induced martensitic transformation is rather challenging for small volume ceramics, as it requires a non-destructive probe, with micro/sub-micro-scale resolution working at elevated temperatures.

To shed light on the thermally-induced martensitic transformation behavior in small volume zirconia, we employed a synchrotron scanning micro X-ray diffraction (μXRD) setup [19,20] equipped with a heating stage. Employing this non-destructive characterization tool that has submicron resolution and microsecond sampling time [21,22], the transformation crystallography of micron-sized zirconia (doped with yttria and titania) was studied *in-situ* as a function of temperature, providing an in-depth understanding of the characteristic martensitic transformation temperatures as well as monoclinic variant preference during transformation.

2. Materials preparation and characteristics

All the micron-sized samples in this work were machined from bulk yttria-titania co-doped zirconia (YTDZ) with a composition of 2 mol% Y_2O_3–5 mol% TiO_2–ZrO_2 (denoted as: $2Y_2O_3$–$5TiO_2$–ZrO_2), into single crystal pillars. The bulk YTDZ ceramics were prepared using a conventional ceramic fabrication procedure, taking a powder → compaction → sintering approach, the details of which were described in our previous work [10]. The surface morphology of the polycrystalline ceramics was characterized with scanning electron microscopy (SEM, equipped with a field emission gun, FEI Nova 600i Nanolab), as shown in Fig. 1(a). The average grain size is 4 μm, which is much larger than the critical size for size stabilization of tetragonal phase (<200 nm) [23,24]. For the micron-sized crystals to be discussed in this work, therefore, only the dopant Y_2O_3 is considered as a tetragonal phase stabilizer. Two micron-sized grains (Grain 1 and Grain 2), as shown in Fig. 1(b), were cut from the bulk YTDZ ceramic using focused ion beam (FIB, FEI Nova 600i Nanolab) and then attached by Pt deposition to a silicon substrate using an Omni-Probe. Two micron-sized pillars (Pillar 3 and Pillar 4) were milled from bulk YTDZ using FIB through a three-step milling procedure. A large crater with a diameter of 40 μm (Fig. 1(c)) was milled at 21 nA to avoid substrate interference on subsequent micromechanical testing, followed by milling to the desired pillar size at 0.92 nA and final polishing at 28 pA (Fig. 1(d)). After mechanical compression, Pillar 3 was cut using FIB and attached to a silicon substrate for μXRD studies, as shown in Fig. 1(e).

To study the thermally-induced martensitic transformation, the micron-sized zirconia samples mounted on Si substrates were scanned with μXRD on Beamline 12.3.2 at the Advanced Light Source, Lawrence Berkeley National Laboratory, Berkeley, CA, with the experimental setup schematically illustrated in Fig. 2(a) [25]. The samples (Grain 1, Grain 2 and Pillar 4) were placed on a customized heating stage atop the instrument stage. Zirconium X-ray fluorescence maps obtained from a silicon drift detector (Vortex-EM, SII Nanotech) were used to precisely locate the zirconia samples with the X-ray beam. Subsequently, Laue diffraction patterns were obtained from a focused polychromatic X-ray beam (5–22 keV) and collected by an area X-ray detector (DECTRIS Pilatus 1 M Pixel array detector). The X-ray beam size was about 0.5 μm × 0.5 μm, and the whole sample was mapped by rastering

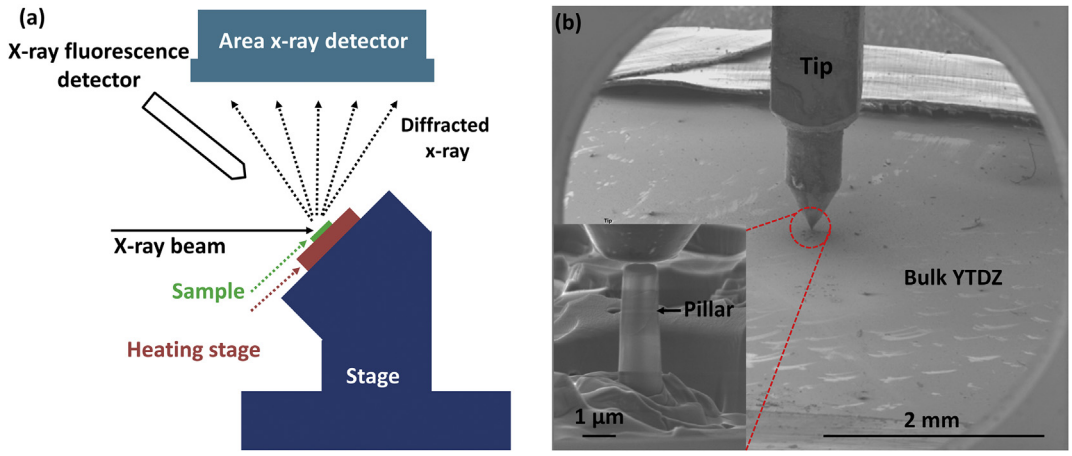

Fig. 2. (a) Schematic illustrations on synchrotron μXRD scanning [25], (b) SEM images taken during *in-situ* micromechanical testing of pillars.

the stage using a step-size of 0.5 μm. The heating stage was controlled to heat the substrate from 25 to 700 °C, followed by subsequently cooling to 25 °C, at intervals of 50 or 100 °C and ramping rates between intervals of ~5 °C/min. At each temperature, the sample was held for 10 min prior to μXRD scanning, to reduce thermal vibration and stabilize the system. The actual temperature on the silicon substrate was systematically calibrated with a thermocouple. The collected Laue diffraction patterns were analyzed to obtain information of crystal phase, orientation and lattice parameter, using the XMAS software package on a supercomputer at NERSC (National Energy Research Scientific Computing Center) [26].

To demonstrate the shape memory effect on pillars at room and high temperatures, Pillar 3 and Pillar 4 (on two separate bulk YTDZ ceramics) were attached to two different *in-situ* nanoindenters housed in SEM chambers, as shown in Fig. 2(b). The details of pillar dimensions and mechanical testing parameters are listed in Table 1. After carefully aligning the tip, both Pillar 3 and Pillar 4 were compressed in a closed-loop load control mode at a loading/unloading rate of 0.2 mN/s. Pillar 4 was attached to the heating stage of the nanoindenter and heated to 400 °C at a rate of 10 °C/min, followed by a 20 min dwell before compression. After compression, the pillar was heated to 650 °C to observe shape recovery.

3. Martensitic transformation in micron-sized zirconia

During the μXRD scanning of micron-sized zirconia, several distinct Laue diffraction patterns were observed, with two examples shown in Fig. 3(a) and (b) for a single sample, at two different temperatures. These two Laue diffraction patterns can be exclusively indexed as tetragonal (Fig. 3(a), with $a = 5.103$ Å, $c = 5.184$ Å [10]) and monoclinic (Fig. 3(b), with $a = 5.160$ Å, $b = 5.222$ Å, $c = 5.323$ Å, $\beta = 99.147°$ [10]) zirconia crystal, respectively; the change between these Laue patterns denotes the phase transformation.

3.1. Pristine zirconia grains

Fig. 4 shows the crystal orientation map of Grain 1 and Grain 2 during a heating/cooling cycle of 25 °C → 550 °C → 133 °C. Each pixel in the map represents a diffraction pattern at a particular position on the grain, which was indexed using both the tetragonal and monoclinic crystals, similar to Fig. 3. A successful indexation of more than 15 peaks in the pattern is considered a valid indexation and denoted with a color that represents a particular crystallographic orientation. In these representations, the color code is used only for the purpose of distinguishing different Laue patterns, and does not have any quantitative correlation to crystallographic orientation. Black is used to denote areas where indexation was unsuccessful. According to Fig. 4 (a) and (b), both grains were composed of a single-crystal tetragonal phase at room temperature. When the temperature was increased, the grains gradually transformed into the monoclinic phase, with no tetragonal phase indexed between 259 °C and 435 °C. Upon transformation, the formerly single-colored grains changed to exhibit binary-colored monoclinic maps, i.e., each individual crystal transformed into two monoclinic variants having different crystallographic orientations, with each variant spanning a few micrometers. Upon further heating to 476 °C, the monoclinic phase started to transform back to the tetragonal phase, with further heating leading to more and more pixels better indexed as tetragonal phase. The phase

Table 1
Parameters for compression tests of YTDZ pillars.

Pillar	Dimension		Test temperature (°C)	Maximum load (mN)	*In-situ* Nanoindenter	Diameter of conductive diamond Tip (μm)
	Effective diameter (μm)	Height (μm)				
3	2.29	5.30	25	12	PI85, Hysitron, housed in FESEM, FEI Nova 600i Nanolab	5
4	3.02	3.62	400	10	PI87 equipped with a heating stage (up to 800 °C), Hysitron, housed in FESEM, FEI Nova 600i Nanolab	10

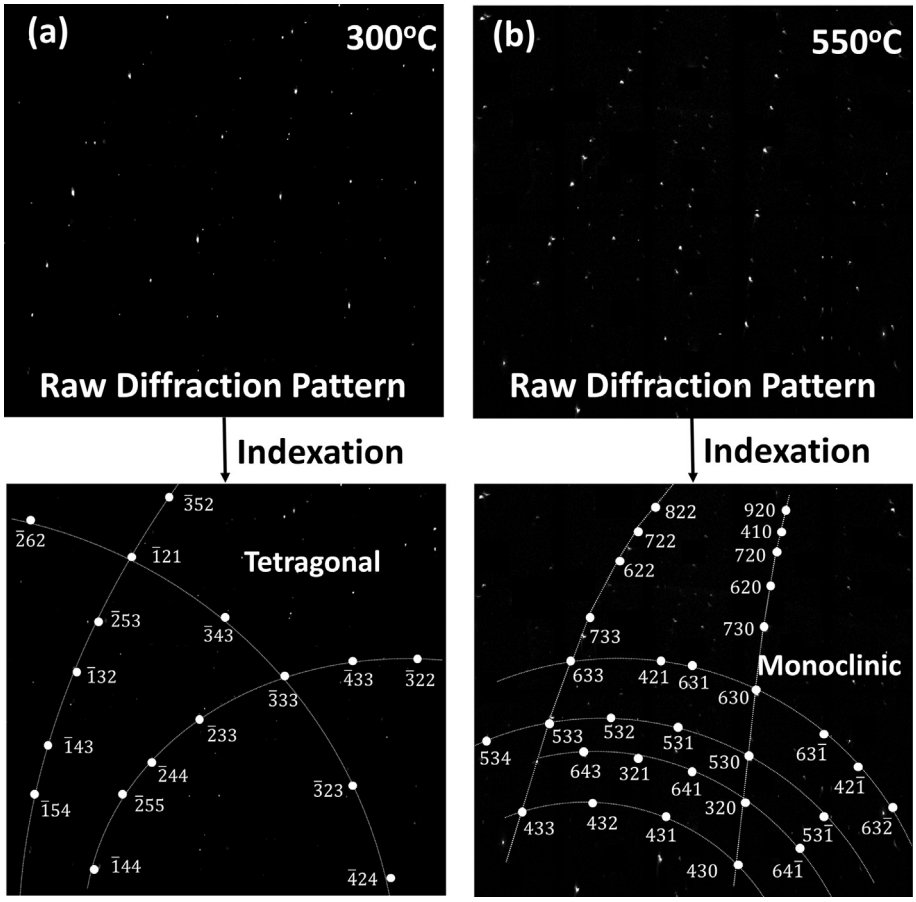

Fig. 3. Two representative Laue diffraction patterns of Grain 1 at (a) 300 °C and (b) 550 °C, together with the corresponding *hkl* indices for the (a) tetragonal and (b) monoclinic phases.

transformation almost completed at 546 °C, with both grains mostly reverted to single crystal tetragonal phase. During cooling, the transformation was reversed, with single crystal tetragonal crystal transforming back to binary monoclinic variants starting at about 397 °C. The grain then remained monoclinic down to room temperature.

Overall, despite their difference in crystallographic orientations, both grains went through three transformation stages during a cycle of heating and cooling. The phase transformations and their characteristic temperatures can be determined quantitatively by calculating the areas of colored pixels on the tetragonal and monoclinic maps in Fig. 4. The calculated phase compositions with respect to the temperature are shown in Fig. 5.

It is noteworthy that there is a seemingly abnormal transformation from tetragonal to monoclinic phase in both grains during the first heating process (25–250 °C). Prior to micromachining, these grains were embedded in a bulk sample during high temperature firing and subsequent cooling, where they experienced mechanical constraint from a surrounding matrix during grain growth. At compositions such as studied here, where the martensitic transformation temperatures are in the vicinity of room temperature, the equilibrium stable phase is very sensitive to such constraint [27]. As a result, it is common to metastably retain the high-temperature tetragonal phase [27,28] down to room temperature, and even to metastably retain it when the constraint is removed; that is exactly what is observed in Figs. 4 and 5. At room temperature the samples begin in the tetragonal phase, and revert to the equilibrium martensite phase upon heating to a temperature sufficient to overcome kinetic barriers to the equilibration, in this case, just over 100 °C or so. The subsequent transformations that are observed are thermodynamic, and characteristic of the expected martensitic transformation.

The four characteristic martensitic transformation temperatures (austenite start and finish, A_s, A_f, and martensite start and finish, M_s, M_f) can be obtained from Fig. 5 for our composition of $2Y_2O_3$–5-TiO_2–ZrO_2. For the austenite reversion transformation (monoclinic → tetragonal) A_s and A_f are 476 °C and 510 °C, respectively, while for forward martensitic transformation (tetragonal → monoclinic) M_s and M_f, are 397 °C and 311 °C, respectively. These characteristic transformation temperatures follow expectations from studies of bulk YTDZ ceramics with related compositions [18]. It is to be noted that there is a slight apparent difference in terms of transformation temperature between the two grains, which may simply be a resolution issue given the sparse nature of our temperature sampling in these experiments. In addition, it is worth noting that the transformation temperatures are sensitive to microstructure; for ceria doped zirconia, a decrease of ~40 °C was reported when the grain size dropped from 5 to 0.8 μm [15]. The grains reported in this work are selected to be around 8 μm so that such grain size effects are minimized.

3.2. Mechanically compressed zirconia pillar

The thermomechanical behavior of Pillar 3 was studied through micromechanical compression at room temperature (refer to

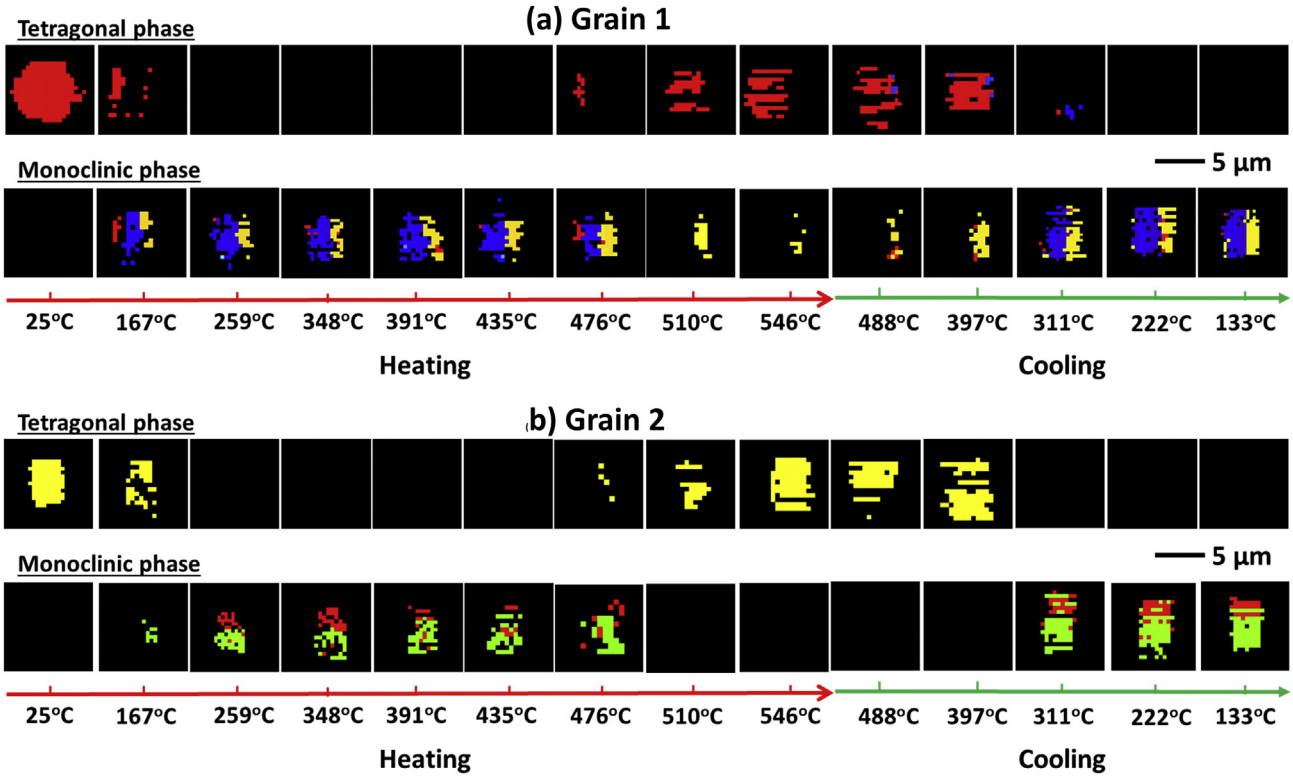

Fig. 4. Crystallographic orientation maps of tetragonal and monoclinic crystals for micron-sized (a) Grain 1 and (b) Grain 2 during a heating/cooling cycle of 25 °C → 550 °C → 133 °C. The exact crystallographic orientations represented by the different colors can be found in Fig. 7(a).

Supplementary Materials), followed by μXRD scanning during heat treatment. The behavior of Pillar 3 under micro-compression is similar to that reported earlier for related materials [10,18], showing significant deformation with signatures of martensitic transformation. A thorough study of the phase transformation was conducted on pre-compressed Pillar 3 using μXRD, by mapping it at different temperatures from 25 to 700 °C, as shown in Fig. 6. It is clear that the pillar experienced partial transformation during compression, as it was composed of a mixture of tetragonal and monoclinic phases at 25 °C before heat treatment. Such partial transformation has been reported earlier in Ref. [18] and can be attributed to the constraint at the regions near the compression tip and substrate. Because Pillar 3 originates from a single crystal tetragonal grain, such partial transformation makes it possible to study the transformation crystallography with more nuance. Only one monoclinic variant was introduced during compression, as seen from the red monoclinic variant at 25 °C, instead of the binary monoclinic variants of the pristine grains. This observation agrees with our earlier work that partial transformation with a single variant is more likely to occur during stress-induced transformation [18].

During heating, the non-stress-transformed domain (tetragonal domain) transformed into a single monoclinic crystal at modest temperatures merely high enough to overcome kinetic constraints on equilibration. This is similar behavior to that of the grains from the as-processed pristine grains, but in this case, the stress-induced monoclinic variant apparently serves as a template for the remaining transformation, because the transformation completes with that same variant consuming the full pillar.

Upon further heating, the austenite reversion transformation in this pillar is strikingly higher, between 650 °C (A_s) and 700 °C (A_f), as compared to the pristine sample (450–500 °C). One of the possible sources for the higher transformation temperatures in stress-transformed specimen is dislocations introduced when the pillar was mechanically compressed. A similar phenomenon has been reported in shape memory alloys, where dislocations can form at the interface between the martensite and austenite domains, hindering the interface movement [29]. As a result, more energy and thus higher temperatures are needed to trigger the reverse transformation [30]. Another contributing factor might be the difference in terms of monoclinic variant preference during the two transformation processes; the uniaxial compression might not favor the same variant correspondence as the unidirectional temperature change, as we will discuss in more detail below. Access to different variants could also lead to possible differences in the transformation temperatures, which may also contribute to the difference in M_s and M_f during cooling. During cooling, the pillar remained a single crystal in the tetragonal phase until about 300 °C, after which the tetragonal volume fraction dropped to zero by 200 °C, showing lower transformation temperatures (by ~ 100 °C) than the pristine grains. Some Laue patterns were successfully indexed as monoclinic from 250 °C (Fig. 8(d)) but no clear monoclinic map was obtained due to thermal drifting and they are not shown here.

4. Transformation crystallography of micron-sized zirconia

4.1. Thermally-induced martensitic transformation

A tetragonal crystal of zirconia can be transformed into a total of 12 possible monoclinic variants [31], including 3 unique correspondences each offering 4 variants. The details of the crystallographic change during thermally-induced martensitic transformation can be directly studied from the maps in Figs. 4 and 6, for both pristine grains and the mechanically compressed pillar. For pristine grains, the specific crystallographic orientations of both

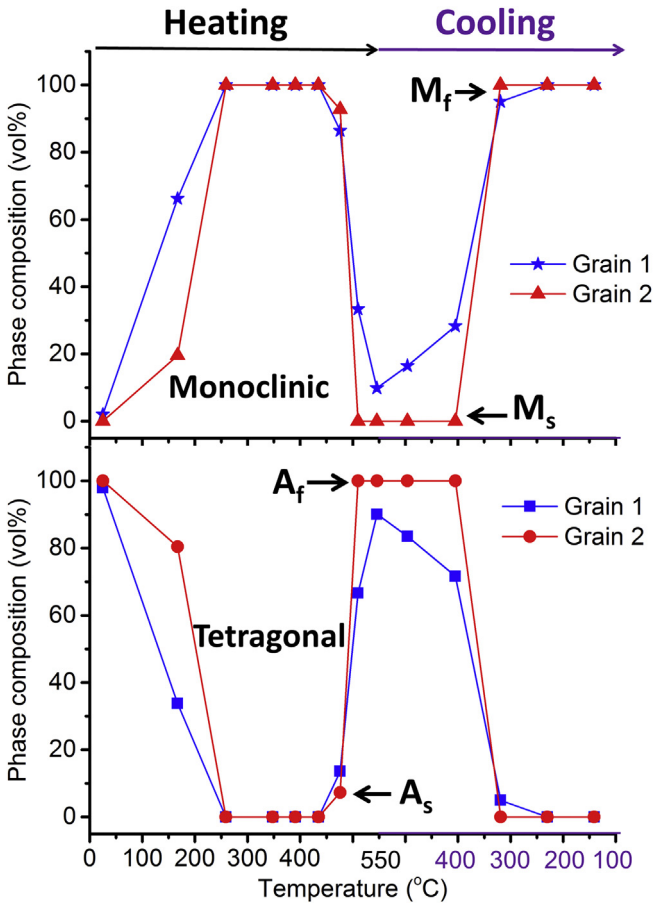

Fig. 5. Normalized phase compositions of the monoclinic and tetragonal phases for Grain 1 and Grain 2 during a heating/cooling cycle of 25 °C → 550 °C → 133 °C.

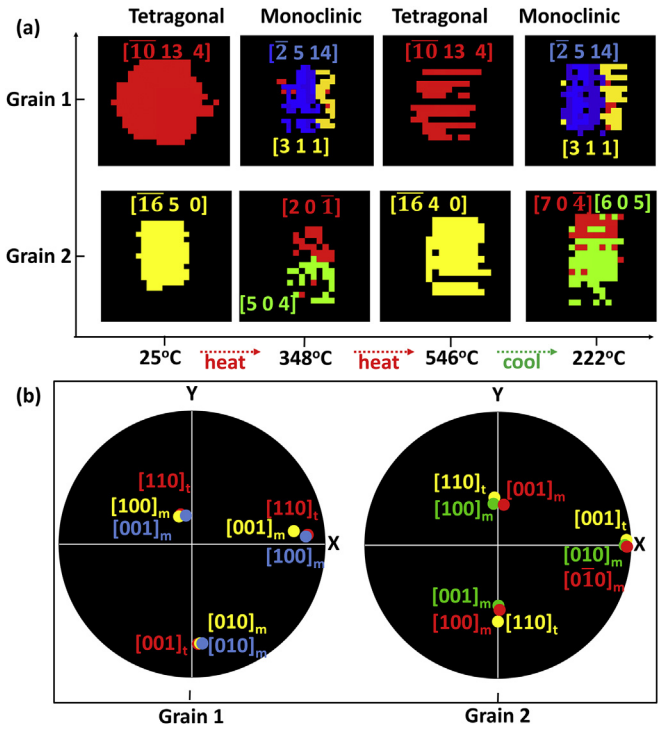

Fig. 7. (a) Crystal orientations of both tetragonal and monoclinic phases at different temperatures for Grain 1 and Grain 2, and (b) corresponding in pole figures for the [100], [010], [001] and [110] axis. The same color was used to denote each crystal in maps in (a) and pole figures in (b).

tetragonal and monoclinic phases are shown in Fig. 7(a). The tetragonal crystals at 25 and 546 °C have the same orientation, while the monoclinic crystals at 435 and 133 °C share the same orientation. Note that these represent conditions separated by a phase transformation cycle, i.e., the same orientations are favored before and after the sample is cycled to the other phase, for both austenite and martensite. Such reversibility is generally considered useful for shape memory materials, as it suggests the possibility of two-way shape memory without the need for external stress-biasing of the variants.

The orientation relationship between the two phases can be clearly illustrated in the pole figures of Fig. 7(b). In both grains, the positions of the tetragonal [001] poles are aligned with the monoclinic [010] poles, suggesting that the transformation occurred according to "correspondence B", i.e. the *c*-axis in tetragonal unit cell becomes the *b*-axis in the transformed monoclinic unit cell, and the axes are related by $[001]_t//[010]_m$. As a result, the equivalent *a* and *b*-axes of the tetragonal crystal become the *a* and *c*-axes of the monoclinic phase, as can be confirmed by the same positions observed on $[110]_t$ and $[100]_m/[001]_m$. This observation agrees with the literature [32] indicating that correspondence B is favored in yttria doped zirconia when the transformation is thermally induced. Although two variants emerge for these grains, they are both of correspondence B, as their poles fall on the same locations, but with their positions exchanged between

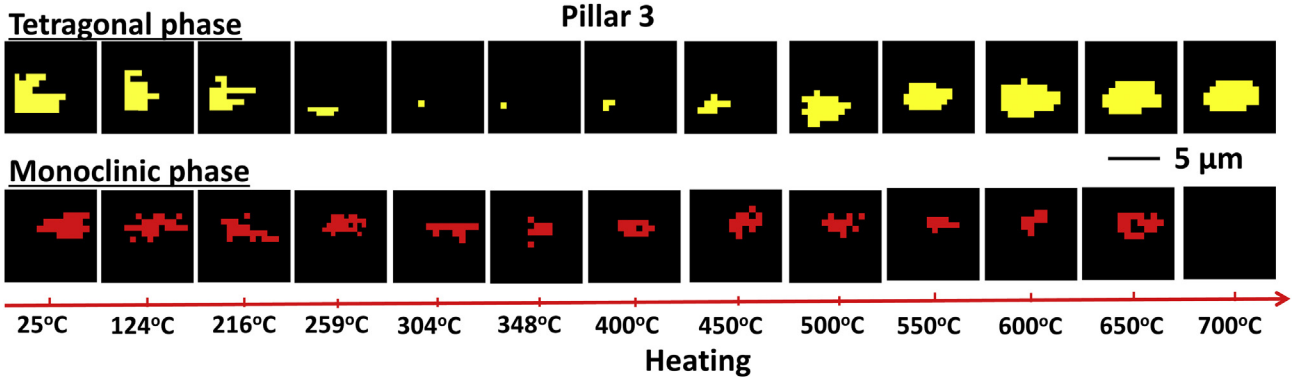

Fig. 6. Crystal orientation maps of tetragonal and monoclinic crystals for Pillar 3 during a heating cycle of 25 °C → 700 °C. The exact crystallographic orientations represented by different colors are indicated in Fig. 8(a).

[100] and [001]. That is, among the four possible variants of correspondence B, the two monoclinic variants of each grain are related by a 90° rotation around [010].

Another interesting observation in Fig. 7 is that there seems to be a specific energetically-favored variant for different positions on the grain. The left section of Grain 1 always transforms into the monoclinic variant with orientation [$\bar{2}$ 5 14] (in blue), whereas the right section always transforms into the variant with orientation [3 1 1] (in yellow); similarly, the top section of Grain 2 always favors the red monoclinic variant whereas the bottom section favors the green. As the two variants in each grain originate from the same tetragonal single crystal, the difference in preferred variants is not likely due to differences in composition, temperature or area-to-volume ratio. There are a few possibilities for this "training" of the structure. First, as is common in most shape memory materials, the defect substructure may favor a specific kinematic pathway and the reproducible formation of these variants. Although these grains were not intentionally mechanically trained, they experienced significant thermal excursions during processing, along with expansion mismatch loading amongst the grains, as well as the transformation itself. There are therefore many sources of dislocation substructure within the grains, and the variant training could be a result of this. Second, it is possible that due to the micro-scale processing of this sample, that other effects bear on the variant training; in small specimens surface energy effects are more significant and could certainly energetically bias variant selection. Similarly, the constraint of our Pt mounting process could affect the strain distribution across the grain and contribute to the difference in the orientation preference of the monoclinic variants.

4.2. Martensitic transformation of pre-strained pillar

The Laue diffraction patterns of Pillar 3 at different stages of heat treatment can be seen in Fig. 8(a)–(d). The monoclinic crystal retains the same orientation of $[1\bar{1}\bar{1}]_m$ through heating from 25 to 650 °C, while the crystal experienced significant lattice distortion through temperature changes as shown in Fig. 8(e). The lattice parameters generally follow a trend that distorts the monoclinic crystal towards a tetragonal one, with ***a/b*** approaching 1, and β decreasing towards 90°. Such lattice distortion persists gradually

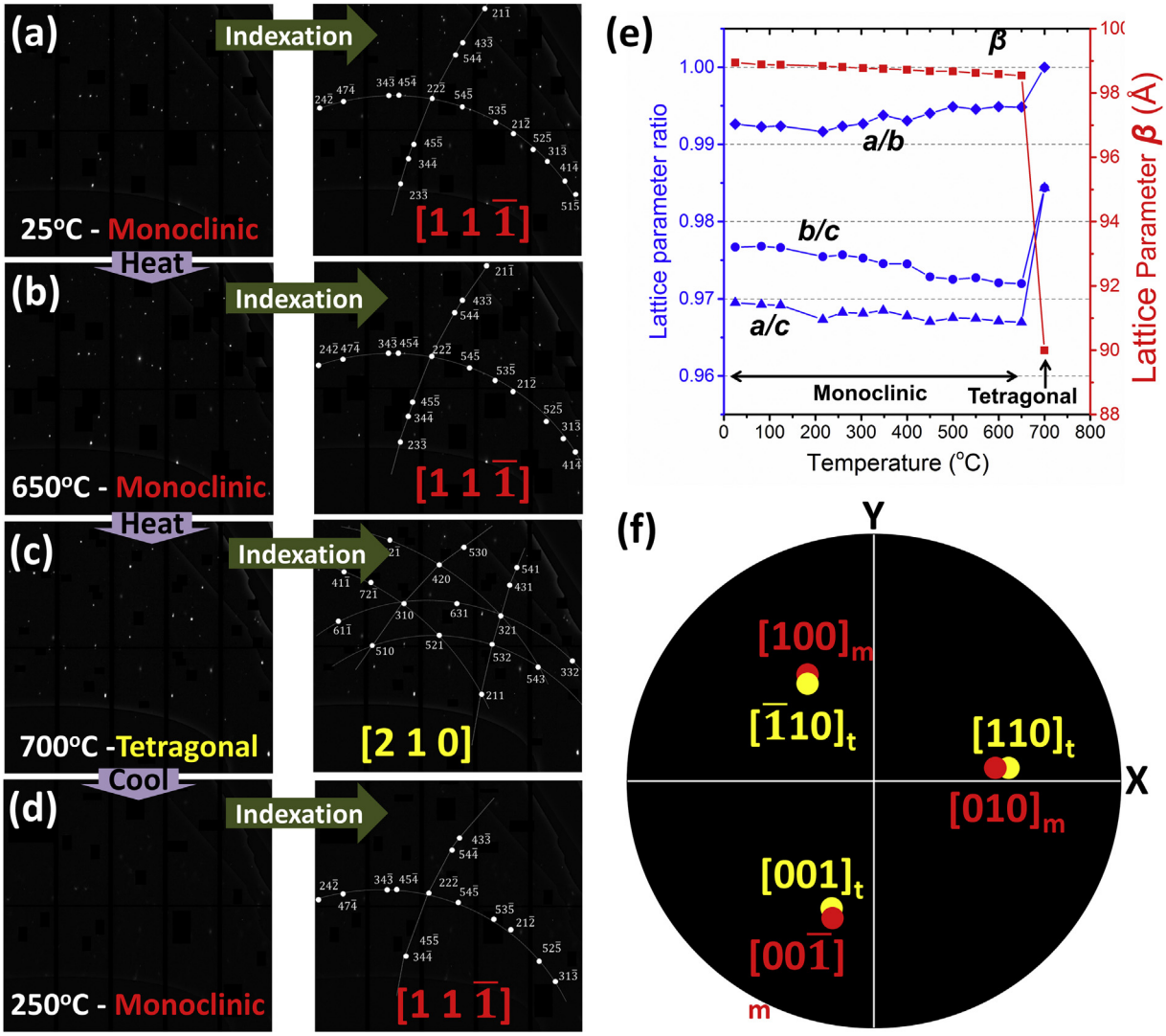

Fig. 8. Laue diffraction patterns of Pillar 4 at (a) 25 °C, (b) 600 °C, (c) 700 °C and (d) 250 °C, with the indexed pattern of monoclinic and tetragonal phase. (e) Lattice parameters for monoclinic and tetragonal crystal (a/b, b/c, a/c and β) during heating of 25 °C → 700 °C. (f) Positions of both monoclinic (red) and tetragonal (yellow) crystals in pole figures from projection axis of [100], [010], [001] and [110]. (For interpretation of the references to colour in this figure legend, the reader is referred to the web version of this article.)

up to 650 °C, above which the reverse martensitic transformation is triggered and proceeds discontinuously. Upon subsequent cooling, the forward transformation occurred at 250 °C, forming a monoclinic crystal with the same orientation as before the heat treatment.

Thanks to the partial transformation during compression, the non-transformed domain can be considered to reflect the initial crystallographic orientation of the metastable tetragonal pillar before compression. By comparing the crystallographic orientations of the non-transformed tetragonal domain with the transformed monoclinic domain in pole figures in Fig. 8(f), the reversible martensitic transformation of Pillar 3 took place according to correspondence C during both mechanical compression and heat treatment, following an orientation relationship of $[100]_t//[100]_m$, $[\bar{1}10]_t//[100]_m$ and $[110]_t//[010]_m$. Thus, stress bias has favored a single monoclinic variant from correspondence C, whereas free-standing grains of similar size tend to transform into binary variants according to correspondence B when triggered by heat. Interestingly, in our prior work on compression-induced transformation, we concluded that correspondence C appeared favored at every orientation with respect to the applied load [18], and found no evidence for correspondence B. The present results are consistent with that observation, but add the interesting complexity that the thermal transformation appears to favor correspondence B instead. The transition between these two transformation paths at intermediate conditions where both thermal and mechanical energy participate significantly in triggering the transformation should present an interesting area for future work.

5. High temperature shape memory effect

Micro-compression at temperatures lower than the austenite start temperature (A_s) can induce shape change via transformation of tetragonal to monoclinic, or de-twinning/rotation of monoclinic variants [16]. This shape change can be subsequently recovered upon heating to the austenite finish temperature (A_f). Based on the above μXRD studies, our zirconia with a composition of $2Y_2O_3$–$5TiO_2$–ZrO_2 has an A_s and A_f of 476 °C and 510 °C, respectively, and can therefore exhibit shape memory potentially at high temperatures up to ~400 °C. The shape memory properties of Pillar 4 were studied at 400 °C through *in-situ* microcompression as shown in Fig. 9. In the load-displacement curve in Fig. 9(f), a large displacement plateau with a maximum uniaxial strain of ~7% was observed during compression, accompanied by clear striped patterns formed on the lateral surface of the as-deformed pillar (Fig. 9(d) and (g)). The large strain originates from de-twinning or rotation of unfavored monoclinic variants into a strain-accommodating favored one, similarly to the shape memory behaviors observed in alloys [33,34].

The original shape was recovered by heating the pillar to 650 °C, and this was accompanied by the disappearance of the striped surface patterns, as seen in Fig. 9(e). It is therefore concluded that for small volume zirconia with composition of $2Y_2O_3$–$5TiO_2$–ZrO_2, shape deformation can be stress-induced at 400 °C and shape recovery can be thermally-induced at 650 °C. The shape recovery temperature of Pillar 4 (650 °C) is consistent with the observed reverse transformation temperature of Pillar 3 (650–700 °C), and both are higher than those in the pristine grains (476 °C–546 °C).

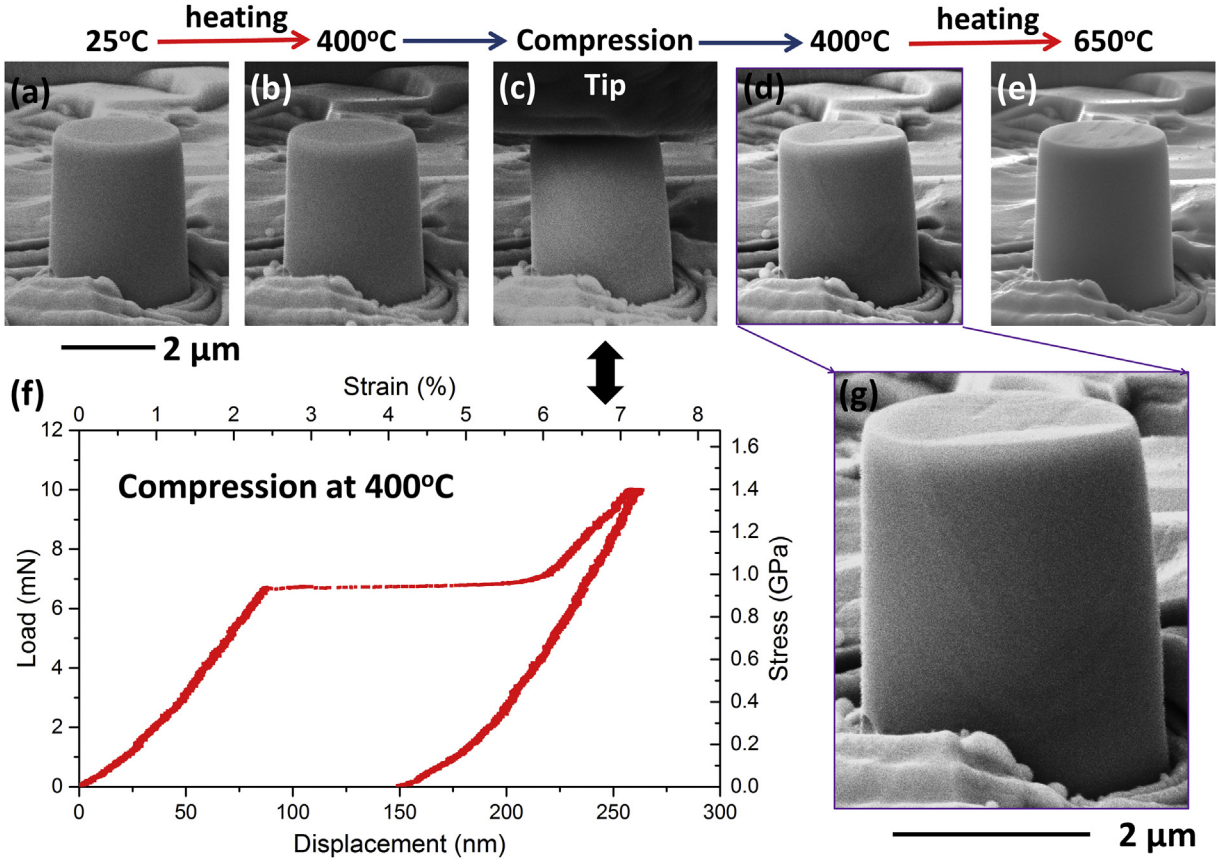

Fig. 9. (a), (b), (c), (d), (e), (g) SEM images of Pillar 4 at different temperatures before and after *in-situ* micromechanical testing (at tilting angle of 12°). (f) Load-displacement (stress-strain) behavior of the pillar at 400 °C.

This demonstration of a full cycle of shape memory with recoverable strain up to 7% in zirconia ceramics at an operation temperature of 400 °C is, so far as we are aware, the first observation of its kind.

This helps to establish that zirconia works as a shape memory material over a wide temperature operation window of at least 375 °C, competitive with many proposed high temperature shape memory alloys [3]. However, the transformation stresses (~1–2.5 GPa) are much higher than for alloys [2], resulting in much higher energies, including actuation energy and damping capacity. Since the martensitic transformation temperature in zirconia is highly tunable through material composition [35] up to 1100 °C, it seems worthwhile to explore shape memory properties of zirconia under a variety of extreme conditions.

6. Conclusion

The martensitic transformation morphology and crystallography has been studied in small volume, micron-scale, zirconia with μXRD. For as-processed pristine ceramics with a composition of $2Y_2O_3$–$5TiO_2$–ZrO_2, the forward martensitic transformation temperatures were determined to be 311 °C (M_f) ~ 397 °C (M_s), with reversion transformation temperatures 476 °C (A_s) ~ 546 °C (A_f). By contrast, prior room temperature compression changes the reversion transformation temperatures, which are higher at 650 °C (A_s) ~ 700 °C (A_f). A closer inspection of the transformation pathways and crystallography revealed some interesting differences between thermally-dominated and mechanically dominated martensitic transformation. The pristine zirconia grains experienced complete transformation according to “correspondence B”, forming binary monoclinic variants that are rotated 90° from each other, but both align the *c-axis* of the tetragonal cell with the *b-axis* of the monoclinic one. On the other hand, uniaxial compression favored monoclinic variants according to correspondence C, and exhibited higher transformation temperatures. Both the transformation temperatures and crystallographic evolution were found to be reversible during transformation, providing the foundation for repeatable two-way shape memory properties, possibly even in the absence of external stress biasing.

Finally, these ceramics displayed the shape memory effect after deformation at both room temperature and a high temperature of 400 °C, as revealed through *in-situ* micromechanical testing. This large operation window and the possibility for composition-tunable transformation temperature, together with properties of high strength and inertness to atmosphere, give zirconia significant potential as an extreme-condition shape memory material.

Acknowledgements

We would like to thank Dr. Alan Lai at MIT for his insightful discussion. We would like to thank Joseph Lefebvre, Ryan J. Stromberg and Ariel Leonard from Hysitron. Inc. for their kind help with high temperature *in-situ* micromechanical tests at Hysitron in Minnesota, USA. The Advanced Light Source (ALS) and the National Energy Research Scientific Computing Center (NERSC) are supported by the Director, Office of Science, Office of Basic Energy Sciences, of the U.S. Department of Energy under Contract No. DE-AC02-05CH11231 at the Lawrence Berkeley National Laboratory (LBNL).

Appendix A. Supplementary data

Supplementary data related to this article can be found at http://dx.doi.org/10.1016/j.actamat.2017.06.006.

References

[1] J.M. Jani, M. Leary, A. Subic, M.A. Gibson, A review of shape memory alloy research, applications and opportunities, Mater. Des. 56 (2014) 1078–1113.
[2] S. Miyazaki, K. Otsuka, Development of shape memory alloys, Isij Int. 29 (1989) 353–377.
[3] J. Ma, I. Karaman, R.D. Noebe, High temperature shape memory alloys, Int. Mater. Rev. 55 (2010) 257–315.
[4] H. Horikawa, S. Ichinose, K. Morii, S. Miyazaki, K. Otsuka, Orientation dependence of β1 → β1′ stress-induced martensitic-transformation in a Cu-Al-Ni alloy, Metall. Trans. A 19 (1988) 915–923.
[5] S. Miyazaki, H.Y. Kim, P.J.S. Buenconsejo, Development of high temperature Ti-Ta shape memory alloys, ESOMAT (2009) 1–8.
[6] A. Nespoli, S. Besseghini, S. Pittaccio, E. Villa, S. Viscuso, The high potential of shape memory alloys in developing miniature mechanical devices: a review on shape memory alloy mini-actuators, Sens. Actuat. A-Phys. 158 (2010) 149–160.
[7] N.B. Morgan, Medical shape memory alloy applications - the market and its products, Mat. Sci. Eng. A-Struct. 378 (2004) 16–23.
[8] D.J. Hartl, D.C. Lagoudas, Aerospace applications of shape memory alloys, P. I. Mech. Eng. G-J. Aer. 221 (2007) 535–552.
[9] A. Lai, Z.H. Du, C.L. Gan, C.A. Schuh, Shape memory and superelastic ceramics at small scales, Science 341 (2013) 1505–1508.
[10] X.M. Zeng, Z.H. Du, C.A. Schuh, N. Tamura, C.L. Gan, Microstructure, crystallization and shape memory behavior of titania and yttria co-doped zirconia, J. Eur. Ceram. Soc. 36 (2016) 1277–1283.
[11] Z.H. Du, X.M. Zeng, Q. Liu, A. Lai, S. Amini, A. Miserez, C.A. Schuh, C.L. Gan, Size effects and shape memory properties in ZrO_2 ceramic micro- and nano-pillars, Scr. Mater. 101 (2015) 40–43.
[12] J.W. Adams, R. Ruh, K.S. Mazdiyasni, Young's modulus, flexural strength, and fracture of yttria-stabilized zirconia versus temperature, J. Am. Ceram. Soc. 80 (1997) 903–908.
[13] E. Carnposilvan, M. Anglada, Size and plasticity effects in zirconia micropillars compression, Acta Mater. 103 (2016) 882–892.
[14] G. Subhash, S. Nematnasser, Dynamic stress-induced transformation and texture formation in uniaxial compression of zirconia ceramics, J. Am. Ceram. Soc. 76 (1993) 153–165.
[15] P.E. Reyesmorel, J.S. Cherng, I.W. Chen, Transformation plasticity of CeO_2-stabilized tetragonal zirconia polycrystals .2. Pseudoelasticity and shape memory effect, J. Am. Ceram. Soc. 71 (1988) 648–657.
[16] J. Chevalier, L. Gremillard, A.V. Virkar, D.R. Clarke, The tetragonal-monoclinic transformation in zirconia: lessons learned and future trends, J. Am. Ceram. Soc. 92 (2009) 1901–1920.
[17] D.M. Owen, A.H. Chokshi, The high temperature mechanical characteristics of superplastic 3 mol% yttria stabilized zirconia, Acta Mater. 46 (1998) 667–679.
[18] X.M. Zeng, A. Lai, C.L. Gan, C.A. Schuh, Crystal orientation dependence of the stress-induced martensitic transformation in zirconia-based shape memory ceramics, Acta Mater. 116 (2016) 124–135.
[19] N. Tamura, R.S. Celestre, A.A. MacDowell, H.A. Padmore, R. Spolenak, B.C. Valek, N.M. Chang, A. Manceau, J.R. Patel, Submicron x-ray diffraction and its applications to problems in materials and environmental science, Rev. Sci. Instrum. 73 (2002) 1369–1372.
[20] M. Kunz, N. Tamura, K. Chen, A.A. MacDowell, R.S. Celestre, M.M. Church, S. Fakra, E.E. Domning, J.M. Glossinger, J.L. Kirschman, G.Y. Morrison, D.W. Plate, B.V. Smith, T. Warwick, V.V. Yashchuk, H.A. Padmore, E. Ustundag, A dedicated superbend x-ray microdiffraction beamline for materials, geo-, and environmental sciences at the advanced light source, Rev. Sci. Instrum. 80 (2009).
[21] N. Tamura, A.A. MacDowell, R.S. Celestre, H.A. Padmore, B. Valek, J.C. Bravman, R. Spolenak, W.L. Brown, T. Marieb, H. Fujimoto, B.W. Batterman, J.R. Patel, High spatial resolution grain orientation and strain mapping in thin films using polychromatic submicron x-ray diffraction, Appl. Phys. Lett. 80 (2002) 3724–3726.
[22] N. Tamura, H.A. Padmore, J.R. Patel, High spatial resolution stress measurements using synchrotron based scanning X-ray microdiffraction with white or monochromatic beam, Mat. Sci. Eng. A-Struct. 399 (2005) 92–98.
[23] T. Chraska, A.H. King, C.C. Berndt, On the size-dependent phase transformation in nanoparticulate zirconia, Mat. Sci. Eng. A-Struct. 286 (2000) 169–178.
[24] R.C. Garvie, The occurrence of metastable tetragonal zirconia as a crystallite size effect, J. Phys. Chem. 69 (1965) 1238.
[25] T.F. Jiang, C.L. Wu, N. Tamura, M. Kunz, B.G. Kim, H.Y. Son, M.S. Suh, J. Im, R. Huang, P.S. Ho, Study of stresses and plasticity in through-silicon via structures for 3D interconnects by X-ray micro-beam diffraction, IEEE. Trans. Device Mater. Reliab. 14 (2014) 698–703.
[26] N. Tamura, XMAS: a versatile tool for analyzing synchrotron X-ray microdiffraction data, in: R. Barabash, G. Ice (Eds.), Strain and Dislocation Gradients from Diffraction: Spatially-Resolved Local Structure and Defects, Imperial College Press, London, 2014, pp. 125–155.
[27] F.F. Lange, Transformation toughening .1. Size effects associated with the thermodynamics of constrained transformations, J. Mater. Sci. 17 (1982) 225–234.
[28] P.F. Becher, M.V. Swain, Grain-size-Dependent transformation behavior in polycrystalline tetragonal zirconia, J. Am. Ceram. Soc. 75 (1992) 493–502.

[29] Y. Liu, Detwinning process and its anisotropy in shape memory alloys, Smart Mater. 4234 (2001) 82–93.
[30] A.R. Pelton, Nitinol fatigue: a review of microstructures and mechanisms, J. Mater. Eng. Perform. 20 (2011) 613–617.
[31] P.M. Kelly, L.R.F. Rose, The martensitic transformation in ceramics - its role in transformation toughening, Prog. Mater. Sci. 47 (2002) 463–557.
[32] F.R. Chien, F.J. Ubic, V. Prakash, A.H. Heuer, Stress-induced martensitic transformation and ferroelastic deformation adjacent microhardness indents in tetragonal zirconia single crystals, Acta Mater. 46 (1998) 2151–2171.
[33] X.Y. Gao, W.M. Huang, Thermomechanical behavior of shape memory alloys under non-proportional load, P. SPIE 4946 (2003) 183–191.
[34] L. Sun, W.M. Huang, Z. Ding, Y. Zhao, C.C. Wang, H. Purnawali, C. Tang, Stimulus-responsive shape memory materials: a review, Mater. Des. 33 (2012) 577–640.
[35] L.C. Brinson, One-dimensional constitutive behavior of shape memory alloys: thermomechanical derivation with non-constant material functions and redefined martensite internal variable, J. Intel. Mat. Syst. Str. 4 (1993) 229–242.